

miR-149-3p Regulates the Switch between Adipogenic and Osteogenic Differentiation of BMSCs by Targeting FTO

Yuan Li,^{3,7} Fan Yang,^{3,7} Manqi Gao,³ Rui Gong,³ Mengyu Jin,³ Tianyi Liu,^{3,6} Yi Sun,⁵ Yutuo Fu,¹ Qi Huang,⁴ Wenwen Zhang,³ Shenzhen Liu,³ Meixi Yu,³ Gege Yan,³ Chao Feng,³ Mingyu He,³ Lai Zhang,³ Fengzhi Ding,³ Wenya Ma,² Zhenggang Bi,¹ Chaoqian Xu,³ Ye Yuan,² Benzhi Cai,² and Lei Yang¹

¹Department of Orthopedics, The First Affiliated Hospital of Harbin Medical University, Harbin 150001, Heilongjiang, China; ²Department of Pharmacy, The Second Affiliated Hospital of Harbin Medical University, Harbin 150086, Heilongjiang, China; ³Department of Pharmacology, The State-Province Key Laboratories of Biomedicine-Pharmaceutics of China, Key Laboratory of Cardiovascular Research, Ministry of Education, College of Pharmacy, Harbin Medical University, Harbin 150081, China; ⁴Department of Pharmacology, Maternal and Children Health Hospital of Guangxi Zhuang Autonomous Region, Nanning 530003, China; ⁵Department of Orthopedics, The Second Affiliated Hospital of Harbin Medical University, Harbin 150086, China; ⁶College of Pharmacy, University of Cincinnati, Cincinnati, OH 45220, USA

Bone marrow-derived mesenchymal stem cells (BMSCs) have been suggested to possess the capacity to differentiate into different cell lineages. Maintaining a balanced stem cell differentiation program is crucial to the bone microenvironment and bone development. MicroRNAs (miRNAs) have played a critical role in regulating the differentiation of BMSCs into particular lineage. However, the role of miR-149-3p in the adipogenic and osteogenic differentiation of BMSCs has not been extensively discovered. In this study, we aimed to detect the expression levels of miR-149-3p during the differentiation of BMSCs and investigate whether miR-149-3p participated in the lineage choice of BMSCs or not. Compared with mimic-negative control (NC), miR-149-3p mimic decreased the adipogenic differentiation potential of BMSCs and increased the osteogenic differentiation potential. Further analysis revealed that overexpression of miR-149-3p repressed the expression of fat mass and obesity-associated (FTO) gene through binding to the 3' UTR of the FTO mRNA. Also, the role of miR-149-3p mimic in inhibiting adipogenic lineage differentiation and potentiating osteogenic lineage differentiation was mainly through targeting FTO, which also played an important role in regulating body weight and fat mass. In addition, BMSCs treated with miR-149-3p anti-miRNA oligonucleotide (AMO) exhibited higher potential to differentiate into adipocytes and lower tendency to differentiate into osteoblasts compared with BMSCs transfected with NC. In summary, our results detected the effects of miR-149-3p in cell fate specification of BMSCs and revealed that miR-149-3p inhibited the adipogenic differentiation of BMSCs via a miR-149-3p/FTO regulatory axis. This study provided cellular and molecular insights into the observation that miR-149-3p was a prospective candidate gene for BMSC-based bone tissue engineering in treating osteoporosis.

INTRODUCTION

Bone marrow-derived mesenchymal stem cells (BMSCs) are pluripotent progenitors that have the potential to differentiate into multiple cell types, such as osteoblasts, chondrocytes, adipocytes, osteocytes, and myoblasts.¹⁻³ General bone homeostasis relies on the balance between osteogenesis and adipogenesis of BMSCs. The imbalance may lead to pathological consequences, including osteoporosis, which is characterized by a decrease in bone mass and an increase in bone marrow fat accumulation.⁴⁻⁶ Osteoporosis affects many people all over the world, especially postmenopausal women and senior citizens. With the growth of a large aging population, osteoporosis has drawn a lot of attention.⁷ Owing to the abundant sources, strong differentiation potential, and easy access, BMSCs are extensively applied for treatment of osteoporosis and other bone-related diseases.^{8,9}

MicroRNAs (miRNAs) have emerged as a class of small single-stranded noncoding RNAs that are approximately 22 nt in length.¹⁰⁻¹² It is well-known that miRNAs regulate some pathways involved in the pathological conditions through binding to the 3' UTR of the target genes.¹³⁻¹⁵ Recently, several miRNAs have been found to be associated with the differentiation of stem cells.¹⁶⁻¹⁸ For example, it is found that miR-194 inhibits the adipogenesis of mesenchymal stem cells (MSCs) by directly regulating

Received 14 February 2019; accepted 7 June 2019;
<https://doi.org/10.1016/j.omtn.2019.06.023>.

⁷These authors contributed equally to this work.

Correspondence: Lei Yang, Department of Orthopedics, The First Affiliated Hospital of Harbin Medical University, Harbin 150001, Heilongjiang, China.

E-mail: yangray83@vip.qq.com

Correspondence: Benzhi Cai, Department of Pharmacy, The Second Affiliated Hospital of Harbin Medical University, Harbin 150086, Heilongjiang, China.

E-mail: caibz@ems.hrbmu.edu.cn



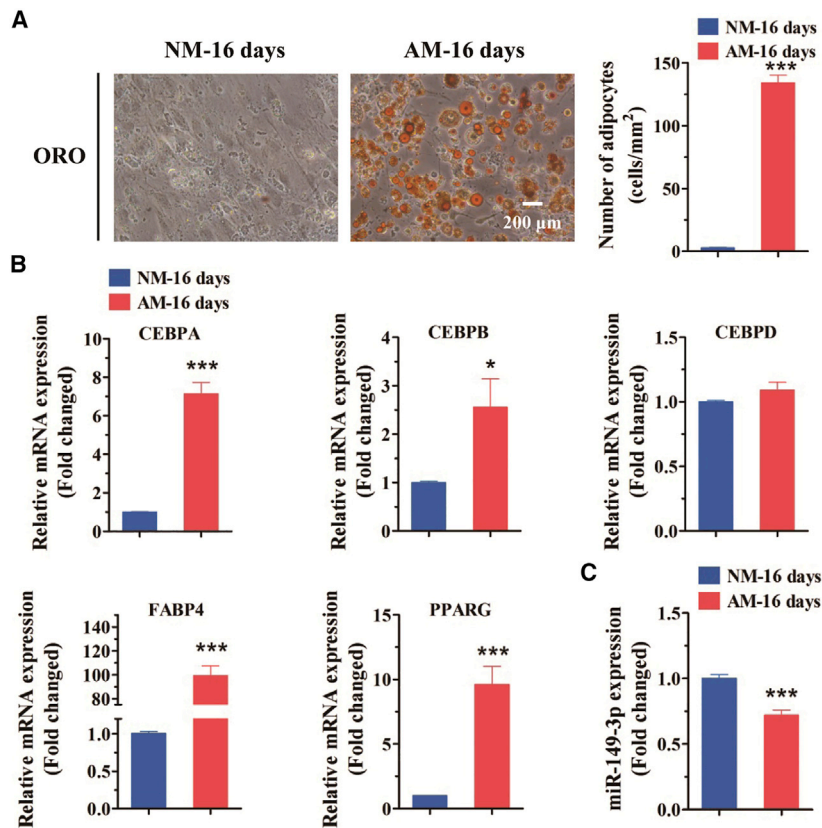


Figure 1. The Expression of miR-149-3p in BMSCs during Adipogenesis

(A) ORO staining was performed to detect the adipogenic differentiation of BMSCs, and quantification analysis of ORO staining was conducted. Scale bar, 200 μ m. (B) Relative mRNA expression of adipocyte marker genes on day 16 of adipogenesis. (C) The expression of miR-149-3p was measured by quantitative real-time PCR analysis during adipogenic differentiation. * $p < 0.05$, ** $p < 0.01$, *** $p < 0.001$. NM, normal culture medium; AM, adipogenic induced medium; CEBPA, CCAAT/enhancer binding protein alpha; CEBPB, CCAAT/enhancer binding protein beta; CEBPD, CCAAT/enhancer binding protein delta; FABP4, fatty acid binding protein 4; PPARG, peroxisome proliferator-activated receptor gamma.

RESULTS

miR-149-3p Is Associated with the Adipogenic Differentiation of BMSCs

BMSCs have the potential to differentiate into multiple cell types under certain conditions. Our previous findings investigated that BMSCs were capable of differentiating into adipocytes in the presence of adipogenic-induced medium (AM).²¹ In the present study, oil red O (ORO) staining was performed for the identification of adipocytes. As shown in the photomicrographs, the number and area of adipocytes were significantly increased in BMSCs after

adipogenic differentiation of 16 days (Figure 1A). We further measured the expression of adipocyte-related genes, including CCAAT/enhancer binding protein alpha (CEBPA), CCAAT/enhancer binding protein beta (CEBPB), CCAAT/enhancer binding protein delta (CEBPD), fatty acid binding protein 4 (FABP4), and peroxisome proliferator-activated receptor gamma (PPARG). The results of quantitative real-time PCR analysis indicated that the expression of these genes was much higher in BMSCs after adipogenesis for 16 days (Figure 1B). The above results suggested that BMSCs had greater adipogenic potential, and they were induced into adipocytes successfully. Quantitative real-time PCR analysis showed that the expression level of miR-149-3p was significantly decreased after adipogenic induction and reduced by about 30% on day 16 (Figure 1C). Taken together, miR-149-3p exhibited dysregulated expression during adipogenesis of BMSCs.

Overexpression of miR-149-3p Inhibits the Adipogenic Differentiation of BMSCs

To mechanistically characterize the effect of miR-149-3p for regulating adipogenesis, we transfected BMSCs with miR-149-3p mimic for subsequent experiments. Quantitative real-time PCR analysis revealed that the expression of miR-149-3p was approximately 13 times higher in BMSCs after transfection of miR-149-3p mimic than its negative control (NC) for 24 h, which

chicken ovalbumin upstream promoter-transcription factor II (COUP-TFII) expression.¹⁹ In addition, miR-135 positively regulates the osteogenic differentiation of adipose-derived stem cells (ADSCs) based on the elevation of bone markers and increase of extracellular matrix calcium deposition through the HOXA2/runt-related transcription factor 2 (RUNX2) pathway.²⁰ Overall, these findings strongly support the crucial functional roles of miRNAs in regulating the differentiation of BMSCs. However, little is known about the regulatory effects of miR-149-3p in regulating the switch between the osteogenic differentiation and adipogenic differentiation of BMSCs.

In this study, we found that miR-149-3p was differentially expressed during adipogenic and osteogenic differentiation of BMSCs. We hypothesized that miR-149-3p might regulate the switch between adipogenesis and osteogenesis of BMSCs. However, the functional roles and mechanism of miR-149-3p in the osteoporosis-induced decreased osteogenic differentiation ability and increased accumulation of fat required further investigation. Therefore, we performed this study to systematically investigate the association between miR-149-3p and differentiation of BMSCs, and to explore the molecular mechanisms involved. This study provided deeper insights into the regulation of BMSC differentiation and presented new effective methods for treating osteoporosis.

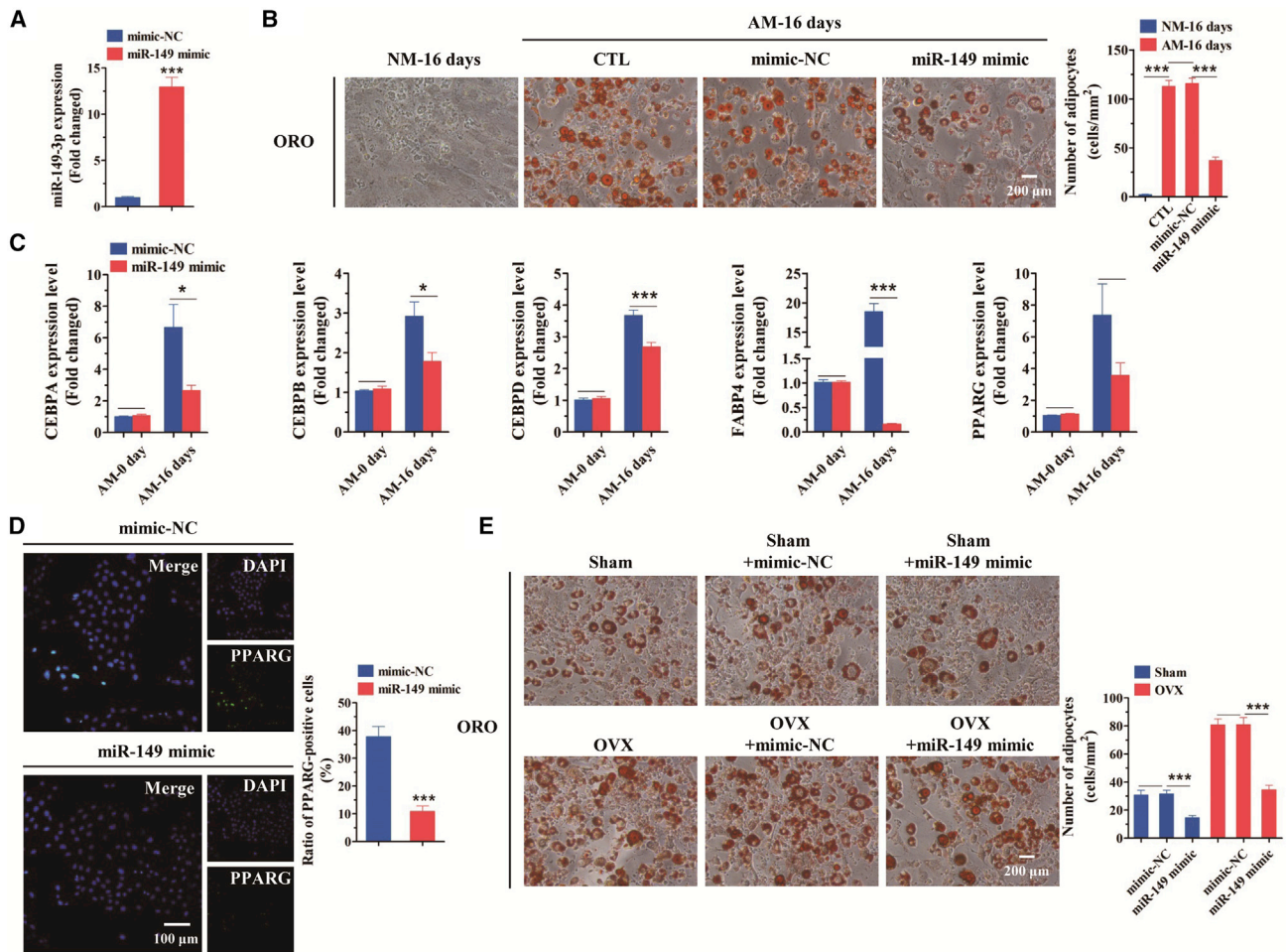


Figure 2. The Effects of miR-149-3p Mimic on Adipogenic Differentiation of BMSCs

(A) The expression level of miR-149-3p in BMSCs after transfection with miR-149-3p mimic. (B) ORO staining was used to test the adipocyte formation in BMSCs treated with miR-149-3p mimic. Histograms showed the quantification of adipocytes. Scale bar, 200 μ m. (C) The relative expression of adipocyte-related genes in BMSCs after transfection of miR-149-3p mimic. (D) Immunofluorescence of PPARG with DAPI counterstaining in mimic-NC, miR-149-3p mimic groups after adipogenic differentiation on day 4. Scale bar, 100 μ m. (E) ORO staining was performed to detect the effects of miR-149-3p mimic on adipogenic differentiation of BMSCs isolated from the Sham or OVX group, and the quantification analysis of ORO staining was shown. Scale bar, 200 μ m. * p < 0.05, *** p < 0.001.

confirmed that miR-149-3p mimic was transfected into BMSCs successfully (Figure 2A). ORO staining demonstrated that miR-149-3p mimic inhibited the lipid droplet formation in BMSCs after adipogenic differentiation for 16 days (Figure 2B). In addition, overexpression of miR-149-3p significantly reduced the expression of the genes associated with adipogenic differentiation, including CEBPA, CEBPB, CEBPD, FABP4, and PPARG (Figure 2C). To assess the effect of miR-149-3p on the expression of the adipocyte-specific gene PPARG during adipogenic differentiation under AM-induced conditions, we transfected BMSCs with miR-149-3p mimic or mimic-NC and cultured them in AM for 4 days. Imaging of the immunofluorescence staining by microscope showed that the number of PPARG-positive cells was reduced after transfection of miR-149-3p mimic in comparison with mimic-NC (Figure 2D).

To further explore whether miR-149-3p regulates the adipogenic differentiation of BMSCs isolated from oophorectomy (OVX)-induced osteoporotic mice, we constructed Sham-operated mouse models or OVX-caused osteoporotic mouse models, respectively. BMSCs were isolated from mice of these two groups and transfected with miR-149-3p mimic or mimic-NC, and ORO-stained cells were imaged using a microscope to measure the adipogenesis of BMSCs after adipogenic differentiation of 16 days. The results uncovered that the adipogenic potential of BMSCs from mice with osteoporosis was stronger than that in the Sham group (Figure 2E). In addition, overexpression of miR-149-3p obviously decreased the adipogenesis of BMSCs in both the Sham and the OVX group (Figure 2E). Therefore, we concluded that overexpression of miR-149-3p effectively attenuated the adipogenic differentiation of BMSCs and inhibited the adipogenesis of BMSCs from osteoporotic mice.

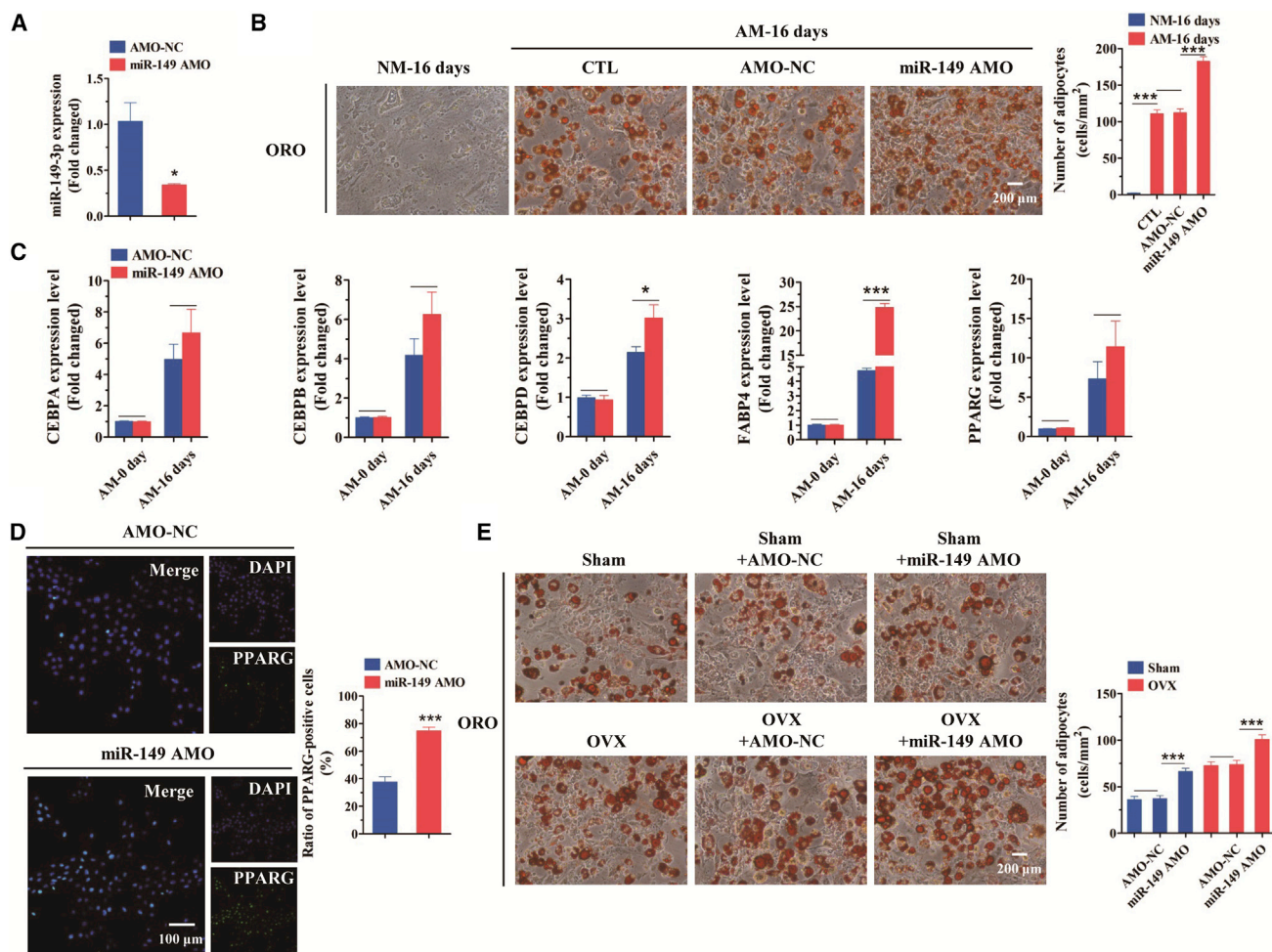


Figure 3. The Roles of miR-149-3p AMO in Adipogenesis of BMSCs

(A) The expression level of miR-149 in BMSCs after transfection with miR-149-3p AMO. (B) The roles of miR-149-3p AMO in the adipogenic differentiation of BMSCs was examined by ORO staining. Scale bar, 200 μ m. (C) The relative expression of adipocyte-related genes was analyzed by quantitative real-time PCR analysis. (D) Immunofluorescence staining analyzed the PPARG-positive BMSCs after transfection of miR-149-3p AMO and AMO-NC. Scale bar, 100 μ m. (E) ORO staining was conducted to determine the effects of miR-149-3p AMO on adipogenic differentiation of BMSCs, which were from the Sham or OVX group. Scale bar, 200 μ m. The quantification analysis of ORO staining also was performed. * $p < 0.05$, ** $p < 0.01$, *** $p < 0.001$.

Knockdown of miR-149-3p Promotes the Adipogenesis of BMSCs

As a second step to study the probable role of miR-149-3p in BMSCs during adipogenesis, we transfected miR-149-3p anti-miRNA oligonucleotide (AMO) into BMSCs for 24 h to knock down miR-149-3p. Also, the expression of miR-149-3p in BMSCs transfected with miR-149-3p AMO was measured using quantitative real-time PCR analysis. The results observed that the expression of miR-149-3p was reduced by approximately 65% after transfection of miR-149-3p AMO (Figure 3A). To further validate the adipocyte differentiation in BMSCs following transfection with miR-149-3p AMO, we performed ORO staining after induction of 16 days. In contrast with the above results, inhibition of miR-149-3p dramatically accelerated the adipogenesis of BMSCs compared with its NC (Figure 3B). As analyzed by quantitative real-time PCR analysis, the expression of adipogenesis-related genes, including CEBPA, CEBPB,

CEBPD, FABP4, and PPARG, was notably enhanced after exposure to miR-149-3p AMO (Figure 3C). Immunofluorescence assay also suggested that transfection of miR-149-3p AMO resulted in an increase in the percentage of PPARG-positive cells, indicating knockdown of miR-149-3p played a positive role in the adipogenesis of BMSCs (Figure 3D). In addition, knockdown of miR-149-3p was able to increase the adipogenic potential of BMSCs (Figure 3E). These results concluded that suppression of miR-149-3p increased the adipogenic capacity of BMSCs.

miR-149-3p Was Involved in the Osteogenic Differentiation of BMSCs

To study whether miR-149-3p was involved in the osteogenic differentiation, we cultured BMSCs in normal culture medium or osteogenic induction medium (OM) for 14 days. Alizarin red S (ARS)

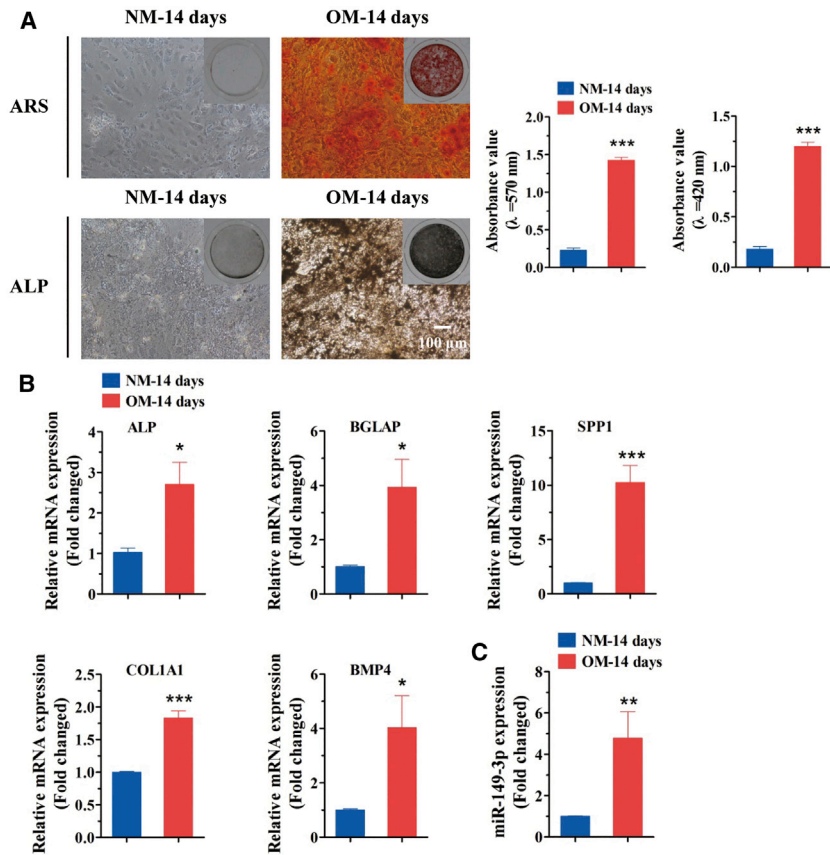


Figure 4. The Expression of miR-149-3p in BMSCs during Osteogenic Differentiation

(A) ARS and ALP stainings were performed on day 14 of osteogenic induction. Scale bar, 100 μ m. (B) Relative expression level of osteoblastic-related genes on day 14 of osteogenic induction. (C) The expression of miR-149-3p was analyzed by quantitative real-time PCR analysis during osteogenesis. * $p < 0.05$, ** $p < 0.01$, *** $p < 0.001$. ALP, alkaline phosphatase; BGLAP, Osteocalcin; SPP1, secreted phosphoprotein 1; COL1A1, collagen type I alpha 1 chain; BMP4, bone morphogenetic protein 4; NM, normal culture medium; OM, osteogenic induced medium.

and alkaline phosphatase (ALP) staining showed that osteogenic induced medium obviously promoted the osteoblastic differentiation of BMSCs, leading to a marked increase in mineralized matrix (Figure 4A). Quantitative real-time PCR analysis supported the notion that osteogenic induced medium improved the expression levels of osteoblast-specific genes, including ALP, Osteocalcin (BGLAP), secreted phosphoprotein 1 (SPP1), collagen type I alpha 1 chain (COL1A1), and bone morphogenetic protein 4 (BMP4) (Figure 4B). To further test the physiological function of miR-149-3p in the osteogenic differentiation, we obtained results about the expression of miR-149-3p during the osteogenesis. Interestingly, the expression of miR-149-3p was about five times higher in BMSCs treated with OM than that in BMSCs cultured in normal culture medium for 14 days, which was consistent with the expected results (Figure 4C). The results strongly suggested that miR-149-3p was upregulated during the osteoblastic differentiation period.

Increasing miR-149-3p Expression Stimulated the Osteogenic Differentiation and Ameliorated the Impaired Osteogenesis of BMSCs in OVX Mice

In order to elucidate the function of miR-149-3p in the differentiation of BMSCs into osteoblasts, we applied ARS and ALP stainings to measure the matrix calcium deposition. As shown in photomicrographs of ARS and ALP stainings, transfection of miR-149-3p mimic greatly

stimulated the osteoblast differentiation of BMSCs, resulting in more calcium depositions compared with mimic-NC (Figure 5A). Moreover, the expression levels of ALP, BGLAP, SPP1, COL1A1, and BMP4, as markers of osteogenic differentiation, were greatly increased after treatment with miR-149-3p mimic, which was displayed by quantitative real-time PCR analysis (Figure 5B). According to the pictures of immunofluorescence, BMSCs transfected with miR-149-3p mimic displayed slightly greater rates of RUNX2-positive cells with its NC (Figure 5C). ARS and ALP stainings indicated that the osteogenic potential of BMSCs isolated from OVX-induced osteoporotic mice was much lower than that from the Sham group (Figure 5D). Further analysis confirmed that overexpression of miR-149-3p could reverse the decrease in the osteogenic differentiation of BMSCs, which was caused by osteoporosis (Figure 5D). It was demonstrated that overexpression of miR-149-3p exhibited significant promotive effects on the osteogenic differentiation of BMSCs.

Knockdown of miR-149-3p Contributed to the Decrease in Osteogenic Differentiation of BMSCs

Then, we treated the cells with miR-149-3p AMO to silence miR-149-3p and provide direct evidence for the role of miR-149 in the osteogenesis of BMSCs. After being transfected with miR-149-3p AMO or AMO-NC, BMSCs were cultured in osteogenic induced medium. After 14 days of osteogenic differentiation, ARS staining indicated that knockdown of miR-149-3p significantly inhibited the osteogenic differentiation of BMSCs (Figure 6A). Furthermore, ALP staining revealed that miR-149-3p AMO suppressed the osteogenesis of BMSCs compared with its NC (Figure 6A). The mRNA expression of osteogenic-specific markers, ALP, BGLAP, SPP1, COL1A1, and BMP4, was also consistently significantly reduced by miR-149-3p AMO after osteogenesis of 14 days (Figure 6B). Immunofluorescence staining showed that when BMSCs were treated with miR-149-3p AMO, the number of RUNX2-positive cells was obviously reduced after osteogenic differentiation of 3 days (Figure 6C). Besides, BMSCs were collected from OVX-induced

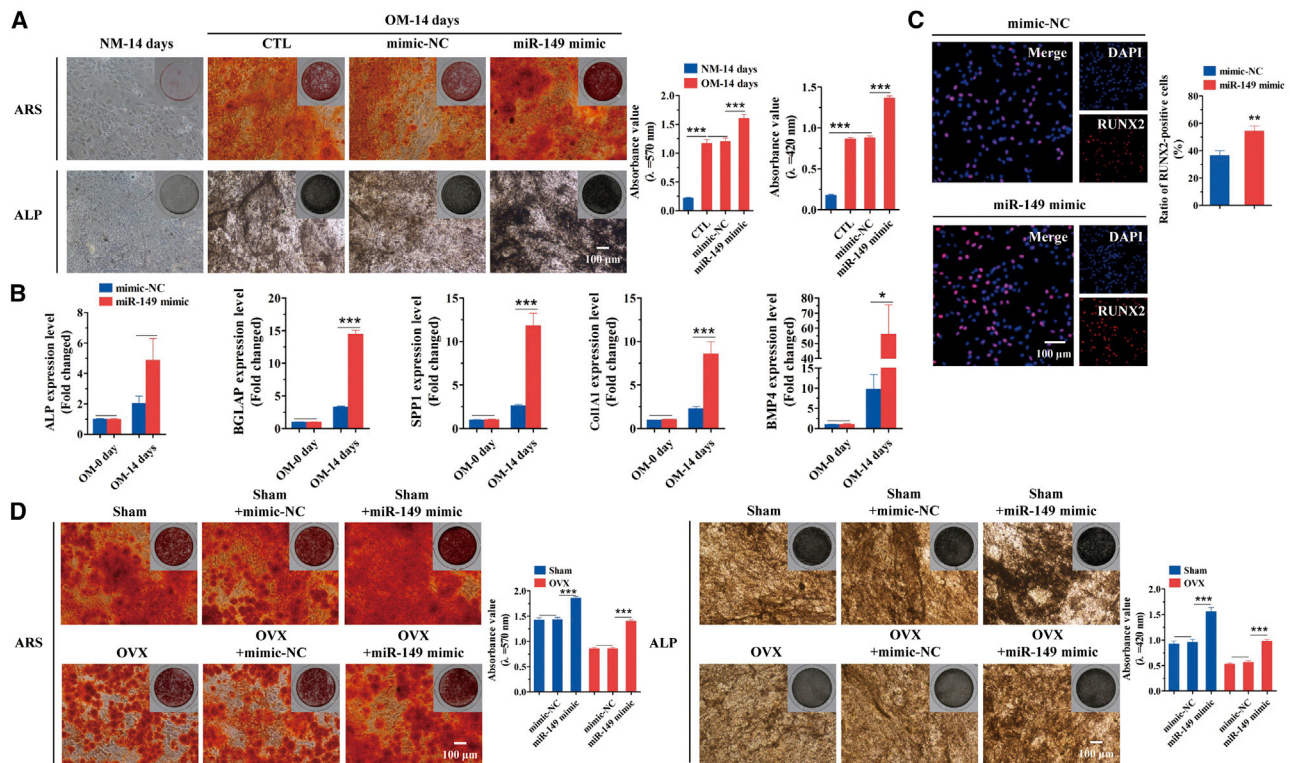


Figure 5. Osteogenesis of BMSCs Was Promoted by miR-149-3p Overexpression

(A) Images and quantification analysis of ARS and ALP stainings in different groups were shown. Scale bar, 100 μ m. (B) Relative mRNA expression of ALP, BGLAP, SPP1, COL1A1, and BMP4 was measured by quantitative real-time PCR analysis in BMSCs after treatment with miR-149-3p mimic. (C) Immunofluorescence was used to determine the role of miR-149-3p mimic in the expression of RUNX2, and the RUNX2-positive cells were counted. Scale bar, 100 μ m. (D) ARS and ALP stainings showed that treatment with miR-149-3p mimic prevented osteoporosis-related decrease in the osteogenesis of BMSCs. Scale bar, 100 μ m. * p < 0.05, *** p < 0.001.

osteoporotic mice and Sham-operated mice, and the BMSCs were induced into osteoblasts (Figure 6D). The results of ARS and ALP stainings demonstrated that knockdown of miR-149-3p further reduced the osteogenesis of BMSCs from osteoporotic mice or control group (Figure 6D). Collectively, the above results indicated that the decrease of miR-149-3p inhibited the differentiation of BMSCs into osteoblasts.

miR-149-3p Regulates the Differentiation of BMSCs by Inhibiting FTO

To further confirm the mechanism about the stimulative effects of miR-149-3p on the osteogenic differentiation and the inhibitory effects of miR-149-3p on the adipogenic differentiation of BMSCs, we performed the bioinformatics analysis. The results showed that the FTO gene, a major adipogenesis-associated regulator, might be a potential target of miR-149-3p (Figure 7A). To clarify the detailed mechanism how miR-149-3p regulated FTO, we established luciferase reporter vectors that contained either a wild-type (WT) FTO 3' UTR or a FTO 3' UTR involving mutant sequences of the miR-149-3p binding site. As shown in Figure 7B, miR-149-3p mimic, but not its AMO, substantially inhibited the luciferase reporter activities elicited by the wild-type FTO 3' UTR (Figure 7B). Furthermore,

the luciferase activities produced by the vector carrying the mutated FTO 3' UTR were not affected by miR-149-3p AMO (Figure 7B). Strikingly, the mRNA level of FTO was significantly downregulated by overexpression of miR-149-3p and upregulated by knockdown of miR-149-3p (Figure 7C). In addition, the protein expression level of FTO was decreased by miR-149-3p overexpression and enhanced by the miR-149-3p knockdown (Figure 7D). Taken together, these results revealed that miR-149-3p directly modulated the adipogenic differentiation of BMSCs by directly targeting FTO.

DISCUSSION

The maintenance of bone homeostasis is mainly dependent on osteoblast-mediated bone formation.^{22,23} BMSCs from patients with osteoporosis exhibit a significant decline in their ability to differentiate into osteoblasts with respect to adipocytes, which lead to progressive bone loss and fat accumulation in bone marrow.^{24,25} However, the mechanism behind this shift of cell lineage commitment of BMSCs requires further investigation.

A subset of miRNAs, including miR-216, miR-146a-5p, miR-26a, miR-29b, etc., have been reported to regulate BMSC lineage commitment

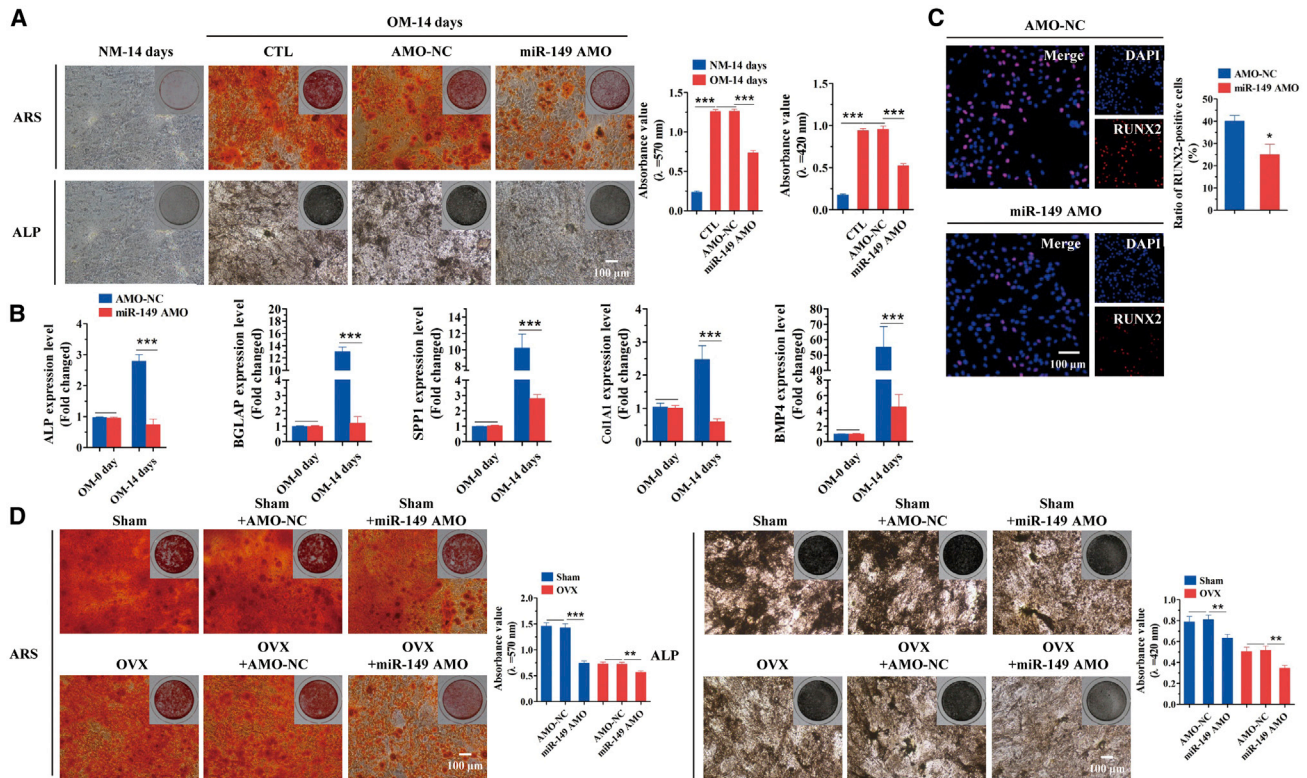


Figure 6. Osteogenic Differentiation of BMSCs Was Inhibited by Knockdown of miR-149-3p

(A) ARS and ALP staining showed that knockdown of miR-149-3p decreased the calcium deposits of BMSCs. Scale bar, 100 μ m. (B) The expression of ALP, BGLAP, SPP1, COL1A1, and BMP4 in BMSCs treated with miR-149-3p AMO was monitored by quantitative real-time PCR analysis. (C) Immunofluorescent assay was used to detect the expression of RUNX2 after transfection of miR-149-3p AMO. Scale bar, 100 μ m. (D) ARS and ALP stainings were performed to detect the role of miR-149 AMO in the osteogenesis of BMSCs collected from the Sham or the OVX group. * $p < 0.05$, ** $p < 0.01$, *** $p < 0.001$.

and play a vital role in bone development.^{26,27} However, whether miRNAs are involved in the development of osteoporosis is probably undiscovered. Based on comprehensive miRNAs profiling, the results uncovered that miR-149-3p was decreased in BMSCs after adipogenic differentiation and increased in BMSCs after osteogenic differentiation. Moreover, consistent with the above results, transfection of miR-149-3p mimic significantly inhibited the adipogenic differentiation of BMSCs isolated from OVX-induced osteoporotic mice. And treatment with miR-149-3p mimic reversed the decrease in osteogenesis of BMSCs caused by osteoporosis, suggesting that miR-149-3p played a crucial role in the osteoporosis.

Recently, several miRNAs, particularly those targeting important regulators of osteogenesis or adipogenesis, have commonly been regarded as important fate determinants of BMSCs. As reported, miR-204 and miR-637 regulate the differentiation of BMSCs by targeting RUNX2 and Sp7 transcription factor (SP7), which are vital transcription factors in bone development.^{28,29} In addition, overexpression of miR-148b regulates the osteogenic differentiation of ADSCs via regulating BMP2.²⁷ The fat mass and obesity-related (FTO) gene, one of critical factors in regulating body weight and fat

mass, has been reported to be involved in common obesity and body mass index.³⁰ FTO is involved in the fat accumulation mainly by regulating the adipogenesis during the process of adipogenesis.³¹ It was reported that inhibition of FTO or mutation in FTO resulted in the reduction of body weight and fat accumulation.^{32,33} In contrast, overexpression of FTO led to the increase in the body weight and fat mass. Our results demonstrated that miR-149-3p regulated the alternative lineages of BMSCs into adipocytes and osteoblasts by directly targeting FTO. The expression of miR-149-3p in BMSCs appeared to be reduced during adipogenic differentiation, whereas it was elevated during osteogenic differentiation. Overexpression of miR-149-3p decreased the number of oil drops and fat accumulation, mainly by inhibiting the adipogenic potential of BMSCs. However, inhibition of miR-149-3p increased the number of adipocytes and promoted the differentiation of BMSCs into adipocytes. Besides, further analysis showed that miR-149-3p played a positive role in the osteogenic differentiation of BMSCs, leading to the increase in the extracellular matrix maturation and mineralization. Our findings revealed that overexpression of miR-149-3p expression in BMSCs might be a new strategy to treat osteoporosis-related abnormal differentiation of BMSCs.

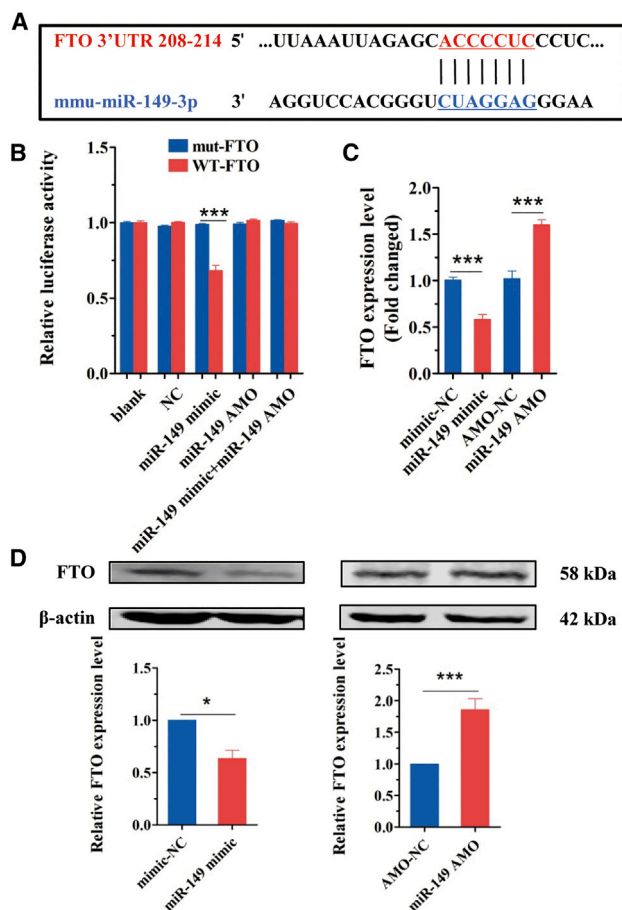


Figure 7. miR-149-3p Regulated the Adipogenesis by Targeting FTO

(A) The binding sites between miR-149-3p and FTO were shown. (B) Luciferase reporter assay was performed to explore the relationship between miR-149-3p and FTO. (C) The mRNA expression of FTO was detected after transfection of miR-149-3p mimic or miR-149-3p AMO. (D) The protein expression of FTO was determined after transfection of miR-149-3p mimic or miR-149-3p AMO. * $p < 0.05$, *** $p < 0.001$.

In conclusion, the current findings revealed the view that the miR-149-3p regulated the BMSC differentiation by inhibiting FTO. Our results suggested a new mechanism of osteoporosis-related imbalance between osteogenesis and adipogenesis, and further provided a novel target for treating osteoporosis.

MATERIALS AND METHODS

BMSC Isolation and Culture

Animal procedures in this study were approved by the Animal Experimental Ethics Committee of Harbin Medical University. Primary mouse BMSCs were isolated from bone marrow by using established approaches described in previous reports.^{21,34} Female C57BL/6J mice (18–20 g) were purchased from the Experimental Animal Center of the Second Affiliated Hospital of Harbin Medical University. Under sterile conditions, the BMSCs were collected by flushing the femurs

and tibias with normal culture medium (NM) (Cyagen Biosciences, USA), which was composed of culture basal medium, 10% fetal bovine serum (FBS), 1% penicillin-streptomycin, and 1% glutamine. The cells were plated in 25-cm² flasks (Nest, China) and cultured at 37°C, 5% CO₂, and in a humidified incubator (Thermo, USA).

Cell Transfection

When the confluence reached 50%–60%, the transfection was performed. Mmu-miR-149-3p mimic, miR-149-3p anti-miRNA oligonucleotide (AMO), and their respective NCs were purchased from GenePharma, China. The sequences of mmu-miR-149-3p mimic were: primary chain, 5'-GAGGGAGGGACGGGGGCGGUGC-3', and passenger chain, 5'-ACCGCCCCGUGCCUCCUCUU-3'. The sequences of mimic-NC were: primary chain, 5'-UUCUCCG AACGUGUCACGUTT-3' and passenger chain, 5'-ACGUGAACA GUUCGGAGAATT-3'. The sequence of mmu-miR-149-3p AMO was: 5'-GCACCGCCCCGUGCCUCCUC-3'. The sequence of AMO-NC was: 5'-CAGUACUUUGUGUAGUACAA-3'. Transfection was performed in the presence of transfection reagent X-treme (Roche, Switzerland) and Opti Reduced Serum Medium (Invitrogen, USA). After transfection for 24 h, the cells were obtained for additional experiments.

Adipogenic Differentiation

For adipogenic differentiation of BMSCs, when the confluence reached 80%–90%, the cells were cultured in adipogenic differentiation medium (AM) (Cyagen Biosciences, USA) for 16 days. AM A consists of 175 mL culture medium, 10% FBS, 1% penicillin-streptomycin, 1% glutamine, 0.1% dexamethasone, 0.2% insulin, 0.1% rosiglitazone, and 0.1% isobutylmethylxanthine (IBMX). AM B was composed of 175 mL culture medium, 10% FBS, 1% glutamine, 1% penicillin-streptomycin, and 0.2% insulin. BMSCs were maintained in AM A for 3 days and then in AM B for 1 day to differentiate into adipocytes.

Osteogenic Differentiation

As for osteogenic induction, the BMSCs were seeded in 6-well or 24-well plates (Nest, China). When BMSCs reached the density of 80%–90%, the BMSCs were grown in the osteogenic induced medium (OM) (Cyagen Biosciences, USA) for 21 days, which contained 10% FBS, 1% glutamine, 0.2% ascorbic acid, 1% penicillin-streptomycin, 0.01% dexamethasone, and 1% β -glycerophosphate to be induced into osteoblasts.

ORO Staining and Quantitative Analysis

ORO staining was performed to detect the lipid droplet formation of BMSCs after adipogenic differentiation. After adipogenesis, the cells were washed by PBS (Solarbio, China) three times. Then, the cells were fixed in 4% paraformaldehyde (PFA) (Solarbio, China) for 30 min at room temperature. After being washed by PBS, the cells were stained by ORO staining dye liquor (Cyagen Bioscience, USA) for 20 min. Finally, 10 pictures were randomly taken by using an inverted optical microscope (Nikon, Japan) for analysis. The adipocytes exhibited the red oil droplets under a microscope. To perform the quantitative analysis, we counted the number of adipocytes per square millimeter (mm²).

ARS Staining and Quantitative Analysis

ARS staining was performed to detect the osteogenesis in BMSCs. In brief, the induced cells were rinsed by PBS and fixed in 4% PFA for 30 min at room temperature. After they were washed by PBS three times, BMSCs were incubated by ARS staining solution (Cyagen Bioscience, USA) for 20–30 min at room temperature. The photomicrographs were randomly taken under an optical microscope (Nikon, Japan). To quantify the degree of mineralization of BMSCs, the cells were washed by PBS and incubated in the presence of 100 mM cetylpyridinium chloride (Sigma, USA) for 1 h. After ARS was solubilized, the absorbance of the released ARS was detected at 570 nm using a microplate reader (TECAN, Switzerland).

ALP Staining and Quantitative Analysis

ALP staining was used to determine the mineralization of BMSCs maintained in the OM or NM, and we performed ALP staining using the method as described previously.²¹ The differentiated cells in 24-well plates were washed by PBS to remove medium, then fixed by 95% ethyl alcohol and stained with ALP staining solution for 4 h in a 37°C incubator followed by several washes with PBS. Then, 2% cobalt nitrate (Tianjin Tianli Chemical Reagents, China) and ammonium sulfide (Tianjin Fuyu Fine Chemical, China) was added into the plates, respectively. Besides, the pictures were captured under an inverted optical microscope (Nikon, Japan). To visualize the calcium deposition, we incubated the cells with 10 mM p-nitrophenyl phosphate (Dalian Meilunbio, China) for 30 min. Finally, the absorbance value ($\lambda = 420$ nm) was measured by using microplate reader.

RNA Isolation and Quantitative Real-Time PCR Analysis

Total RNAs were extracted from cells by using TRIzol Reagent (Invitrogen, USA). A NanoDrop spectrophotometer (Thermo, USA) was applied to analyze the quantity and quality of RNAs. Then, 0.5 μ g RNAs from each sample was reverse transcribed into cDNAs using the High Capacity cDNA Reverse Transcription Kit (Applied Biosystems, USA). The condition was: 95°C for 10 min, 2 cycles at 37°C for 1 h, 85°C for 5 min, and cooling at 4°C. The expression of target genes was measured by quantitative real-time PCR analysis using SYBR Green Master reagents (Roche, Switzerland), double-distilled water, primers, and synthesized cDNAs. The condition was as follows: denaturation at 95°C for 10 s, 40 cycles at 95°C for 10 s and 60°C for 30 s. The expression level of genes was analyzed by U6 or glyceraldehyde-3-phosphate dehydrogenase (GAPDH) for normalization. The relative expression of target genes was assessed by the $2^{-\Delta\Delta CT}$ approach. The sequences of primers used for quantitative real-time PCR amplification were listed subsequently in Table 1.

Immunofluorescence Staining

To observe the expression level of osteogenic-related genes and adipogenic-related genes of BMSCs, we conducted immunofluorescence staining according to the standard protocols. First, cells grown on sterile glass coverslips were washed by PBS gently. After fixation by 4% PFA for 30 min at room temperature, the cells were permeabilized

by 0.4% Triton X-100 (Biosharp, China) for 30 min and blocked in the presence of 5% normal goat serum (Biosharp, China) for 30 min. Next, the cells were incubated with primary antibodies against RUNX2 (1:1,000; Abcam, UK) or PPARG (1:1,000; Abcam, UK) at 4°C overnight with gentle shaking. Then, the cells were incubated with the specified secondary antibodies for 1 h at room temperature in a dark room. Finally, the nuclei were counterstained with DAPI (Solarbio, China). Images were captured with a fluorescence microscope (Olympus, Japan) equipped with proper filters. Images were captured in 10 randomly chosen fields in each group.

Establishment of Osteoporotic Mice

All animal experimental procedures were in compliance with the Ethics Committee of Harbin Medical University. Forty-eight C57BL/6J mice (8 weeks old, 18–20 g) were randomly assigned to the Sham group (n = 24) or the OVX group (n = 24). The mice from the OVX group received bilateral ovariectomy surgery, whereas the mice from the Sham group were subjected to excision of fat tissue near the ovaries after anesthetization. After 4 weeks, osteoporotic mouse models were successfully established.

Luciferase Reporter Analysis

The putative miR-149-3p recognition sites in the anti-FTO 3' UTR were predicted by TargetScan 7.2 (http://www.targetscan.org/vert_72/). The FTO 3' UTR reporter plasmid and the mutant form were cloned via using the 3' UTR region of the psiCHECKTM vector (Promega, USA). The reporter vector together with the control or experimental miR-149-3p mimic or miR-149-3p AMO was transfected into cells when the cells reached 50%–60% confluence. The cells were collected after 48 h to assess the relative luciferase activities of the firefly and renilla luciferase using a Dual Luciferase Reporter assay (Promega, USA) as described by the manufacturer's instructions.

Western Blot

Quantitative analysis on the change of protein expressions was conducted by western blot analysis according to the previous reports.^{35,36} After transfection and induction, the cells were harvested for western blotting analysis. The cells were incubated by radioimmunoprecipitation assay (RIPA) lysis buffer (Beyotime, China) at 4°C for 30 min to extract total proteins. Then, approximately 60 μ g of total cell lysates was separated by SDS-PAGE and transferred to a polyvinylidene fluoride (PVDF) membrane (Millipore, USA). The membranes were blocked with 5% non-fat milk for 2 h and immunoblotted overnight at 4°C with anti-FTO (Abcam, UK) or anti- β -actin (ZSGB-BIO, China). Membranes were then incubated with secondary antibodies for 1 h at room temperature in a dark room. The blotted bands were visualized using Image Studio software (Alias, USA).

Statistical Analysis

All data in this work were expressed as mean \pm SEM from at least three replicates for each experiment. Comparisons between two groups were performed using the Student's unpaired t test by the

Table 1. The Primer Sequences Used for Quantitative Real-Time PCR

Primers	Classification	Sequence (5'-3')
Alkaline phosphatase (ALP)	F	ACAACCTGACTGACCCTTCG
	R	TCATGATGTCCGTGGTCAAT
Osteocalcin (BGLAP)	F	TTCTGCTCACTCTGCTGACC
	R	TTTGTAGGCGGTCTCAAGC
Secreted phosphoprotein 1 (SPP1)	F	ACACTTCACTCCAATCGTCC
	R	TGCCCTTCCGTTGTTGTCC
Collagen type I alpha 1 chain (COL1A1)	F	CAGCCGCTTCACCTACAGC
	R	TTTTGTATTCAATCACTGTCTTGCC
Bone morphogenetic protein 4 (BMP4)	F	TCGTTACCTCAAGGGAGTGG
	R	ATGCTGGGACTACGTTTGG
CCAAT/enhancer binding protein alpha (CEBPA)	F	GTGTGCACGCTATGCTAAACCA
	R	GCCGTTAGTGAAGAGTCTCAGTTTG
CCAAT/enhancer binding protein beta (CEBPB)	F	TGGACAAGCTGAGCGACGAG
	R	GAACAAGTTCGCGAGGGTGC
CCAAT/enhancer binding protein delta (CEBPD)	F	CACGACTCCTGCCATGTACG
	R	GCCGCTTGTGGTTGCTGTT
Fatty acid binding protein 4 (FABP4)	F	TTCTGTGCTGCGGGTATT
	R	GATGCCTTGTGGGAACCTGG
Peroxisome proliferator-activated receptor gamma (PPARG)	F	TCACAAGAGGTGACCCAATG
	R	CCATCCTTCACAAGCATGAA
Glyceraldehyde-3-phosphate dehydrogenase (GAPDH)	F	CATCACTGCCACCCAGAAGAC
	R	CCAGTGAGCTTCCGTTTCAG
miR-149-3p	F	CGGGCGAGGGAGGGACGGGG
	R	CAGCCACAAAAGAGCACAAAT
	RT	CCTGTTGTCTCCAGCCACAAAAGAGCACAAAT ATTCAGGAGACAACAGG
RNA, U6 small nuclear (U6)	F	GCTTCGGCAGCACATATACTAAAAT
	R	CGCTTCACGAATTTGCGTGTTCAT
	RT	CGCTTCACGAATTTGCGTGTTCAT

F, forward; R, reverse; RT, reverse transcription.

GraphPad prism software (GraphPad Software, USA). A value of $*p < 0.05$, $**p < 0.01$, and $***p < 0.001$ was considered statistically significant.

AUTHOR CONTRIBUTIONS

L.Y. and B.C. designed the experiments and finished the manuscript. Y.L., F.Y., M.G., and R.G. performed the cell culture, miRNA transfection, ALP staining, ARS staining, ORO staining, quantitative real-time PCR analysis, and immunofluorescence. M.J. and T.L. performed quantitative real-time PCR analysis and RNA extraction. C.F., Y.S., and Y.F. performed the western blot analysis and animal experiments. Q.H., W.Z., S.L., M.Y., G.Y., M.H., L.Z., and F.D. performed the cell culture, osteogenic induction, and adipogenic induction. W.M., Z.B., C.X., and Y.Y. contributed to the data collection and revised the manuscript.

CONFLICTS OF INTEREST

The authors declare no competing interests.

ACKNOWLEDGMENTS

This work was supported by grants from the National Natural Science Foundation of China (81501920/81573434/81800784), the Postdoctoral Science Foundation of China (2018M630370), the Heilongjiang Postdoctoral Fund (LBH-Z17134), and University Nursing Program for Young Scholars with Creative Talents in Heilongjiang Province (UNPYSCT-2015034).

REFERENCES

- Li, K.C., Chang, Y.H., Yeh, C.L., and Hu, Y.C. (2016). Healing of osteoporotic bone defects by baculovirus-engineered bone marrow-derived MSCs expressing MicroRNA sponges. *Biomaterials* 74, 155–166.

2. Chen, X., Zhi, X., Wang, J., and Su, J. (2018). RANKL signaling in bone marrow mesenchymal stem cells negatively regulates osteoblastic bone formation. *Bone Res.* 6, 34.
3. Cai, B., Li, X., Wang, Y., Liu, Y., Yang, F., Chen, H., Yin, K., Tan, X., Zhu, J., Pan, Z., et al. (2013). Apoptosis of bone marrow mesenchymal stem cells caused by homocysteine via activating JNK signal. *PLoS ONE* 8, e63561.
4. Guo, Q., Chen, Y., Guo, L., Jiang, T., and Lin, Z. (2016). miR-23a/b regulates the balance between osteoblast and adipocyte differentiation in bone marrow mesenchymal stem cells. *Bone Res.* 4, 16022.
5. Lv, Y.J., Yang, Y., Sui, B.D., Hu, C.H., Zhao, P., Liao, L., Chen, J., Zhang, L.Q., Yang, T.T., Zhang, S.F., and Jin, Y. (2018). Resveratrol counteracts bone loss via mitofilin-mediated osteogenic improvement of mesenchymal stem cells in senescence-accelerated mice. *Theranostics* 8, 2387–2406.
6. Qi, M., Zhang, L., Ma, Y., Shuai, Y., Li, L., Luo, K., Liu, W., and Jin, Y. (2017). Autophagy Maintains the Function of Bone Marrow Mesenchymal Stem Cells to Prevent Estrogen Deficiency-Induced Osteoporosis. *Theranostics* 7, 4498–4516.
7. Wu, J.Y., Aarnisalo, P., Bastepe, M., Sinha, P., Fulzele, K., Selig, M.K., Chen, M., Poulton, I.J., Purton, L.E., Sims, N.A., et al. (2011). Gsz enhances commitment of mesenchymal progenitors to the osteoblast lineage but restrains osteoblast differentiation in mice. *J. Clin. Invest.* 121, 3492–3504.
8. Shang, F., Ming, L., Zhou, Z., Yu, Y., Sun, J., Ding, Y., and Jin, Y. (2014). The effect of licochalcone A on cell-aggregates ECM secretion and osteogenic differentiation during bone formation in metaphyseal defects in ovariectomized rats. *Biomaterials* 35, 2789–2797.
9. Liu, Y., Ming, L., Luo, H., Liu, W., Zhang, Y., Liu, H., and Jin, Y. (2013). Integration of a calcined bovine bone and BMSC-sheet 3D scaffold and the promotion of bone regeneration in large defects. *Biomaterials* 34, 9998–10006.
10. Zhao, X.F. (1989). [The synergistic effect of low-dose cyclosporine and fluocinolone acetonide on the survival of rat allogenic skin graft]. *Zhonghua Wai Ke Za Zhi* 27, 495–497, 510.
11. Panizo, S., Naves-Díaz, M., Carrillo-López, N., Martínez-Arias, L., Fernández-Martín, J.L., Ruiz-Torres, M.P., Cannata-Andía, J.B., and Rodríguez, I. (2016). MicroRNAs 29b, 133b, and 211 Regulate Vascular Smooth Muscle Calcification Mediated by High Phosphorus. *J. Am. Soc. Nephrol.* 27, 824–834.
12. Bartel, D.P. (2018). Metazoan MicroRNAs. *Cell* 173, 20–51.
13. Yang, D., Du, G., Xu, A., Xi, X., and Li, D. (2017). Expression of miR-149-3p inhibits proliferation, migration, and invasion of bladder cancer by targeting S100A4. *Am. J. Cancer Res.* 7, 2209–2219.
14. Ding, H., Zheng, S., Garcia-Ruiz, D., Hou, D., Wei, Z., Liao, Z., Li, L., Zhang, Y., Han, X., Zen, K., et al. (2016). Fasting induces a subcutaneous-to-visceral fat switch mediated by microRNA-149-3p and suppression of PRDM16. *Nat. Commun.* 7, 11533.
15. Grigelioniene, G., Suzuki, H.I., Taylan, F., Mirzamohammadi, F., Borochowitz, Z.U., Ayturk, U.M., Tzur, S., Horemuzova, E., Lindstrand, A., Weis, M.A., et al. (2019). Gain-of-function mutation of microRNA-140 in human skeletal dysplasia. *Nat. Med.* 25, 583–590.
16. Wüst, S., Dröse, S., Heidler, J., Wittig, I., Klockner, I., Franko, A., Bonke, E., Günther, S., Gärtner, U., Boettger, T., and Braun, T. (2018). Metabolic maturation during muscle stem cell differentiation is achieved by miR-1/133a-mediated inhibition of the Dlk1-Dio3 mega gene cluster. *Cell Metab* 27, 1026–1039.e6.
17. Zhang, B., Nguyen, L.X.T., Li, L., Zhao, D., Kumar, B., Wu, H., Lin, A., Pellicano, F., Hopcroft, L., Su, Y.L., et al. (2018). Bone marrow niche trafficking of miR-126 controls the self-renewal of leukemia stem cells in chronic myelogenous leukemia. *Nat. Med.* 24, 450–462.
18. Lechman, E.R., Gentner, B., Ng, S.W., Schoof, E.M., van Galen, P., Kennedy, J.A., Nucera, S., Cicceri, F., Kaufmann, K.B., Takayama, N., et al. (2016). miR-126 Regulates Distinct Self-Renewal Outcomes in Normal and Malignant Hematopoietic Stem Cells. *Cancer Cell* 29, 214–228.
19. Jeong, B.C., Kang, I.H., Hwang, Y.C., Kim, S.H., and Koh, J.T. (2014). MicroRNA-194 reciprocally stimulates osteogenesis and inhibits adipogenesis via regulating COUP-TFII expression. *Cell Death Dis.* 5, e1532.
20. Xie, Q., Wang, Z., Zhou, H., Yu, Z., Huang, Y., Sun, H., Bi, X., Wang, Y., Shi, W., Gu, P., and Fan, X. (2016). The role of miR-135-modified adipose-derived mesenchymal stem cells in bone regeneration. *Biomaterials* 75, 279–294.
21. Yang, F., Yang, L., Li, Y., Yan, G., Feng, C., Liu, T., Gong, R., Yuan, Y., Wang, N., Idiattullina, E., et al. (2017). Melatonin protects bone marrow mesenchymal stem cells against iron overload-induced aberrant differentiation and senescence. *J. Pineal Res.* 63, e12422.
22. Wang, L., Niu, N., Li, L., Shao, R., Ouyang, H., and Zou, W. (2018). H3K36 trimethylation mediated by SETD2 regulates the fate of bone marrow mesenchymal stem cells. *PLoS Biol.* 16, e2006522.
23. van Tok, M.N., van Duivenvoorde, L.M., Kramer, I., Ingold, P., Pfister, S., Roth, L., Blijdorp, I.C., van de Sande, M.G.H., Taurrog, J.D., Kolbinger, F., and Baeten, D.L. (2019). Interleukin-17A inhibition diminishes inflammation and new bone formation in experimental spondyloarthritis. *Arthritis Rheumatol* 71, 612–625.
24. Mastrogiacomo, M., Papadimitropoulos, A., Cedola, A., Peyrin, F., Giannoni, P., Pearce, S.G., Alini, M., Giannini, C., Guagliardi, A., and Cancedda, R. (2007). Engineering of bone using bone marrow stromal cells and a silicon-stabilized tricalcium phosphate bioceramic: evidence for a coupling between bone formation and scaffold resorption. *Biomaterials* 28, 1376–1384.
25. Chen, S., Jia, L., Zhang, S., Zheng, Y., and Zhou, Y. (2018). DEPTOR regulates osteogenic differentiation via inhibiting MEG3-mediated activation of BMP4 signaling and is involved in osteoporosis. *Stem Cell Res. Ther.* 9, 185.
26. Hsieh, J.Y., Huang, T.S., Cheng, S.M., Lin, W.S., Tsai, T.N., Lee, O.K., and Wang, H.W. (2013). miR-146a-5p circuitry uncouples cell proliferation and migration, but not differentiation, in human mesenchymal stem cells. *Nucleic Acids Res.* 41, 9753–9763.
27. Liao, Y.H., Chang, Y.H., Sung, L.Y., Li, K.C., Yeh, C.L., Yen, T.C., Hwang, S.M., Lin, K.J., and Hu, Y.C. (2014). Osteogenic differentiation of adipose-derived stem cells and calvarial defect repair using baculovirus-mediated co-expression of BMP-2 and miR-148b. *Biomaterials* 35, 4901–4910.
28. Huang, J., Zhao, L., Xing, L., and Chen, D. (2010). MicroRNA-204 regulates Runx2 protein expression and mesenchymal progenitor cell differentiation. *Stem Cells* 28, 357–364.
29. Zhang, J.F., Fu, W.M., He, M.L., Wang, H., Wang, W.M., Yu, S.C., Bian, X.W., Zhou, J., Lin, M.C., Lu, G., et al. (2011). MiR-637 maintains the balance between adipocytes and osteoblasts by directly targeting Osterix. *Mol. Biol. Cell* 22, 3955–3961.
30. Loos, R.J., and Bouchard, C. (2008). FTO: the first gene contributing to common forms of human obesity. *Obes. Rev.* 9, 246–250.
31. Rivera, M., Cohen-Woods, S., Kapur, K., Breen, G., Ng, M.Y., Butler, A.W., Craddock, N., Gill, M., Korszun, A., Maier, W., et al. (2012). Depressive disorder moderates the effect of the FTO gene on body mass index. *Mol. Psychiatry* 17, 604–611.
32. Gulati, P., Cheung, M.K., Antrobus, R., Church, C.D., Harding, H.P., Tung, Y.C., Rimmington, D., Ma, M., Ron, D., Lehner, P.J., et al. (2013). Role for the obesity-related FTO gene in the cellular sensing of amino acids. *Proc. Natl. Acad. Sci. USA* 110, 2557–2562.
33. Ho, A.J., Stein, J.L., Hua, X., Lee, S., Hibar, D.P., Leow, A.D., Dinov, I.D., Toga, A.W., Saykin, A.J., Shen, L., et al.; Alzheimer’s Disease Neuroimaging Initiative (2010). A commonly carried allele of the obesity-related FTO gene is associated with reduced brain volume in the healthy elderly. *Proc. Natl. Acad. Sci. USA* 107, 8404–8409.
34. Yang, F., Yan, G., Li, Y., Han, Z., Zhang, L., Chen, S., Feng, C., Huang, Q., Ding, F., Yu, Y., et al. (2016). Astragalus polysaccharide attenuated iron overload-induced dysfunction of mesenchymal stem cells via suppressing mitochondrial ROS. *Cell. Physiol. Biochem* 39, 1369–1379.
35. Cai, B., Ma, W., Ding, F., Zhang, L., Huang, Q., Wang, X., Hua, B., Xu, J., Li, J., Bi, C., et al. (2018). The Long Noncoding RNA CAREL Controls Cardiac Regeneration. *J. Am. Coll. Cardiol.* 72, 534–550.
36. Ma, Y., Ma, W., Huang, L., Feng, D., and Cai, B. (2015). Long non-coding RNAs, a new important regulator of cardiovascular physiology and pathology. *Int. J. Cardiol.* 188, 105–110.